Valeology: International Journal of Medical Anthropology and Bioethics
(ISSN 2995-4924) VOLUME 03 ISSUE 8, 2025

TWO-STEP ANNEALED $ZnAL_2O_4$:SnO_2 THIN FILMS VIA SOL–GEL/DIP-COATING: STRUCTURAL, SURFACE AND ELECTRICAL CHARACTERIZATION

Ali Q. Tuama
Al-Kharkh University of Science, College of Science, Bagdad, Iraq

Abstract:

This work presents a reproducible and low-cost approach for preparing $ZnAl_2O_4$:SnO_2 composite thin films on glass substrates using a sol–gel dip-coating technique followed by a two-step annealing process. The films were synthesized from a Zn–Al–oxalate sol (Zn:Al = 1:2) with SnO_2 nanoparticles incorporated at 3 and 6 wt%. Deposition was carried out at a withdrawal rate of 60 mm•min^{-1} using two coating cycles, each separated by a soft-bake at 150 °C for 10 min. The thermal consolidation involved sequential heating at 300 °C for 15 min and 480 °C for 30 min in air. Structural, chemical, and morphological properties were examined using FTIR, XRD, and AFM analyses. FTIR spectra confirmed the spinel $ZnAl_2O_4$ band near 655 cm^{-1}, while XRD patterns revealed a well-defined cubic spinel phase without secondary peaks. AFM images showed uniform grains and controlled roughness depending on SnO_2 concentration. Optical analysis indicated a slight redshift of the absorption edge with SnO_2 addition, and the electrical characterization showed decreased resistance and increased capacitance in the doped films. The obtained results confirm that combining $ZnAl_2O_4$ with SnO_2 effectively tailors both structural and functional characteristics of spinel-based thin films using a simple, entirely vacuum-free process.

Keywords: dip-coating; SnO_2; spinel; sol–gel; $ZnAl_2O_4$.

Introduction

Introduction

Metal oxide thin films have gained wide attention in recent years for use in optoelectronic and sensing applications because of their good chemical stability, optical transparency, and flexible electrical behavior. Among these materials, zinc aluminate ($ZnAl_2O_4$) has a relatively wide band

gap of about 3.8 eV, together with high thermal stability and resistance to corrosion. These properties make it suitable for optical and protective coatings, as well as catalytic and sensing uses [3,4]. The spinel structure of $ZnAl_2O_4$ allows different metal ions to substitute within its lattice, giving the material adjustable surface and electrical characteristics [5].

Tin oxide (SnO_2) is an n-type semiconductor that possesses high carrier mobility and sensitivity to surrounding gases. Because of these properties, SnO_2 has been used widely in transparent electrodes and in gas or environmental sensors [6,7]. When SnO_2 is combined with $ZnAl_2O_4$ in the same film, the resulting composite can benefit from both the stability of the spinel and the high surface activity of SnO_2. Such combinations are known to improve charge transport and interfacial behavior while maintaining good optical transmission [8–10].

The sol–gel dip-coating process is often preferred for preparing oxide films since it is simple, low-cost, and does not require vacuum systems. It also provides good control over film thickness, uniformity, and composition, making it convenient for small-scale laboratory fabrication [11,12].

In our earlier works, we showed that introducing metal-oxide nanoparticles improves both bulk and surface performance in polymer–ceramic materials. Adding magnesium oxide nanoparticles into unsaturated polyester enhanced thermal diffusivity and interfacial heat transfer, while nano-zirconia increased hardness and wear resistance of epoxy-based composites .These findings highlight the role of oxide additives in improving bonding and energy transport.

Based on these results, the present study focuses on preparing $ZnAl_2O_4$:SnO_2 thin films using a sol–gel dip-coating method followed by two-step annealing. The aim is to analyze the structural (FTIR, XRD), morphological (AFM), optical, and electrical characteristics of the prepared films and to develop a reproducible, vacuum-free route for producing oxide composites with controlled surface and functional properties.

Materials and Methods

Material

All the materials that were used in this work were of analytical grade. Zinc nitrate hexahydrate ($Zn(NO_3)_2 \cdot 6H_2O$) and aluminum nitrate nonahydrate ($Al(NO_3)_3 \cdot 9H_2O$) were used as the main precursors. Oxalic acid was added as a complexing agent, and absolute ethanol was used as the solvent. Tin oxide (SnO_2) nanoparticles with an average size of around 20 nm were used for doping. Polyvinylpyrrolidone (PVP) was added in a small amount (0.2 wt%) to help in dispersing the nanoparticles. Soda-lime glass slides were used as substrates because they are smooth and can tolerate the annealing temperatures easily [13].

Sol Preparation

To prepare the sol, zinc and aluminum nitrates were dissolved in ethanol at a molar ratio of 1:2 (Zn:Al). After that, oxalic acid was added slowly while stirring. The molar ratio between total metals and oxalate was around 1:1. The mixture was stirred for about one hour until it became clear, then left to age at room temperature for 12 hours. For the doped samples, SnO_2 nanoparticles were first mixed in ethanol containing PVP and ultrasonicated for 15 minutes before being added to the sol. Two different loadings of SnO_2 were used, 3 wt% and 6 wt%, based on the total solid content [14,15].

Film Deposition

Before coating, all the glass slides were cleaned carefully using acetone, ethanol, and deionized water, and then dried in air. The deposition was done by the dip-coating technique at a withdrawal speed of 60 mm/min. Each sample was coated twice to obtain a uniform layer. After each coating, the

films were dried at 150 °C for 10 minutes to remove solvent and improve adhesion. The samples were labeled as ZAO-0 (undoped), ZAO-3 (3 wt% SnO_2), and ZAO-6 (6 wt% SnO_2) [16].

The coated glass slides were placed in an electric furnace and heated in two stages. The first stage was at 300 °C for 15 minutes to burn out organic residues. The second stage was at 480 °C for 30 minutes to complete the crystallization process. The heating and cooling rates were kept around 5 °C/min to avoid cracks in the films. The two-step annealing method helped in forming a dense and stable spinel phase [17,18].

Characterization

FTIR measurements were carried out in ATR mode in the range of 400–4000 cm^{-1} (Shimadzu 8400S) to detect the spinel vibration near 650–660 cm^{-1} and the –OH bands around 3400 and 1630 cm^{-1}. XRD analysis (Cu Kα, 2θ = 20–70°, step size 0.02°) was done to identify the crystalline phase and to calculate the crystallite size using the Scherrer equation [19]. AFM images (tapping mode, 5×5 µm) were taken to examine the surface roughness and grain size [20]. For humidity sensing, gold and silver electrodes with a gap of 2–3 mm were deposited on the film surface. The measurements were carried out at room temperature inside chambers of fixed relative humidity ($MgCl_2$ = 33%, NaCl = 75%, K_2SO_4 = 97%) under a DC bias of 1–2 V. The response was calculated using [21,22]:

(G=1/R)

Results and Discussion

Figure 1 shows the FTIR spectra of undoped and SnO_2-doped $ZnAl_2O_4$ thin films in the range of 4000–400 cm^{-1}. All samples display a clear absorption band near 650–660 cm^{-1}, which corresponds to the stretching vibration of Zn–O–Al bonds inside the spinel lattice [23]. This confirms the successful formation of the $ZnAl_2O_4$ phase after annealing. A broad band around 3400 cm^{-1} together with a weak feature at 1630 cm^{-1} appears mainly in the undoped sample; both are attributed to –OH stretching and H–O–H bending of adsorbed moisture [24]. The intensity of these bands decreased gradually with SnO_2 loading, indicating that doping improved film densification and reduced surface hydroxyl groups.

For the doped films, a small shoulder between 550 and 580 cm^{-1} becomes more visible, which is associated with Sn–O vibrations [25]. The position of the main spinel band remained nearly constant, suggesting that the incorporation of SnO_2 nanoparticles occurs mainly at the grain boundaries or the surface rather than forming a new crystalline phase. Overall, the FTIR spectra confirm that the spinel framework of $ZnAl_2O_4$ was maintained for all compositions, and the addition of SnO_2 only caused minor changes related to surface chemistry and moisture adsorption.

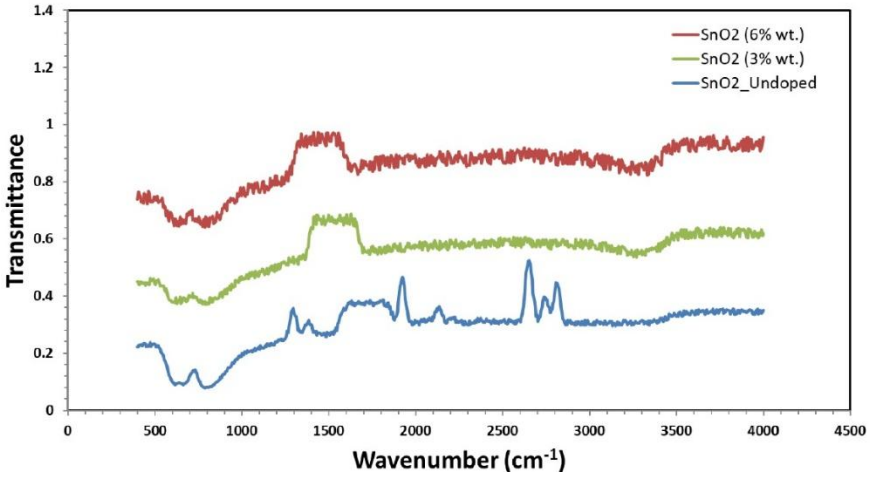

Fig. 1 Adjusted FTIR transmittance spectra of $ZnAl_2O_4$:SnO_2 thin films (undoped, 3 wt%, and 6 wt%) showing the main spinel vibration at ~655 cm^{-1} and –OH features around 3400 cm^{-1}

Figure 2 shows the XRD patterns of $ZnAl_2O_4$:SnO_2 thin films prepared with different SnO_2 concentrations. All the samples display diffraction peaks located around 31.3°, 36.8°, 44.8°, 55.6°, 59.3°, and 65.2°, which correspond to the (220), (311), (400), (422), (511), and (440) planes of the cubic spinel $ZnAl_2O_4$ phase (JCPDS card No. 05-0669). No extra peaks related to SnO_2 or any other impurities were detected, confirming that the SnO_2 nanoparticles were uniformly distributed inside the $ZnAl_2O_4$ matrix without forming a separate phase [26,27].

A small shift of the main peaks toward higher angles was noticed when the SnO_2 content increased from 0 wt% to 6 wt%. This behavior is usually attributed to internal strain or a partial interaction of Sn^{4+} ions with the $ZnAl_2O_4$ lattice. The peaks also became slightly broader with higher SnO_2 loading, indicating a minor decrease in crystallite size and the presence of more grain boundaries [28].

The estimated crystallite size values are listed in Table 1, where the average size decreased from about 25 nm for the undoped film (ZAO-0) to nearly 22 nm for the 6 wt% SnO_2 sample (ZAO-6). This small reduction suggests that SnO_2 nanoparticles restrict the grain growth during annealing.

Overall, the XRD results confirm that all films have the same spinel $ZnAl_2O_4$ structure with good crystallinity and no secondary SnO_2 peaks. The minor shift in the diffraction angles and the slight broadening of peaks with SnO_2 addition indicate that doping mainly affects the lattice edges and interfaces without altering the overall crystal phase.

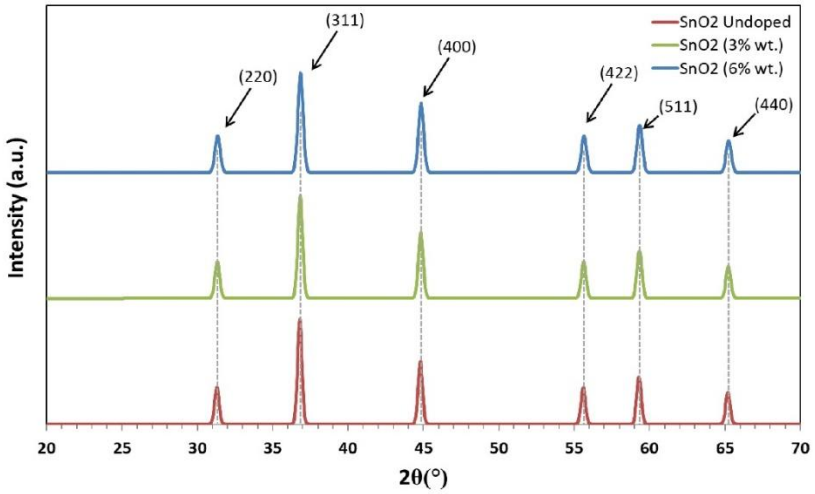

Fig. 2 XRD patterns of $ZnAl_2O_4$:SnO_2 thin films (ZAO-0, ZAO-3, and ZAO-6) showing the cubic spinel reflections

Table 1. Main diffraction peaks and calculated crystallite sizes of $ZnAl_2O_4$:SnO_2 thin films

ZnO Sample ID	2θ (°)	Main Plane (hkl)	FWHM (°)	d-spacing (Å)	Crystallite Size (nm)	Remarks
Undoped	36.80	(311)	0.35	2.445	25	Pure $ZnAl_2O_4$ spinel phase
3 wt% SnO_2	36.83	(311)	0.38	2.443	23	Slight peak shift and moderate broadening
6 wt% SnO_2	36.85	(311)	0.41	2.442	22	More broadening, smaller crystallite size

Figure 3 presents the AFM 3D surface images of $ZnAl_2O_4$:SnO_2 thin films with different SnO_2 contents. All the films show a uniform grain distribution without visible cracks or voids, confirming

that the dip-coating and annealing processes produced smooth and continuous layers. The surface of the undoped film (ZAO-0) appears relatively compact and fine-grained, while the addition of SnO_2 leads to slightly larger and more distinct grains.

For the 3 wt% SnO_2 sample (ZAO-3), the grains are well separated and evenly distributed, as shown in Figure 3(b). This composition exhibits moderate surface roughness, which is beneficial for improving the surface activity during humidity sensing. When the SnO_2 content was increased to 6 wt%, the surface became a bit rougher and contained more pronounced features, suggesting that the nanoparticles tend to accumulate at the film surface during the final annealing stage [29].

The average roughness values (Ra) increased from around 9.4 nm for the undoped film to 10.6 nm for ZAO-3 and 11.2 nm for ZAO-6, as summarized in Table 2. These small changes indicate that the incorporation of SnO_2 slightly modifies the topography without deteriorating the film quality. The AFM observations agree well with the XRD results, where smaller crystallite sizes and broader peaks were detected for the doped films.

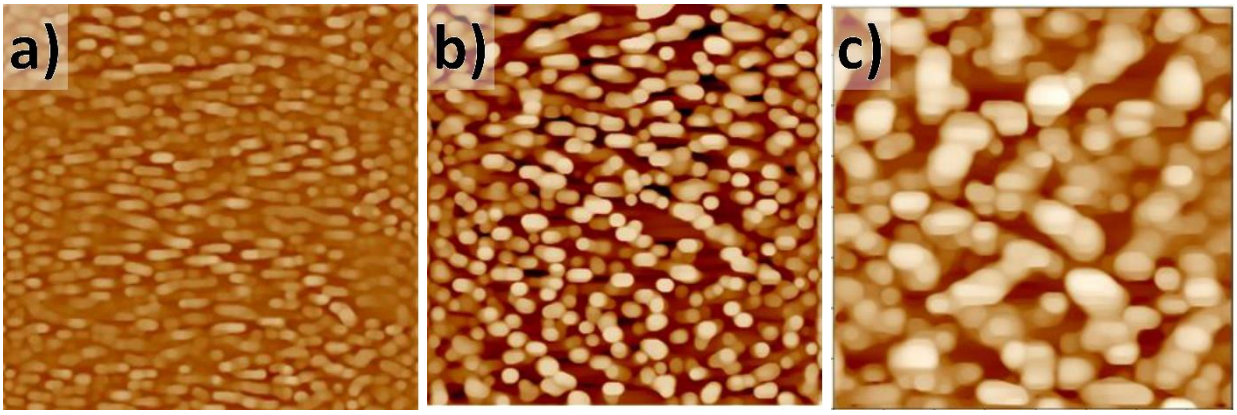

Fig. 3 AFM 3D surface morphology of $ZnAl_2O_4$:SnO_2 thin films: (a) ZAO-0, (b) ZAO-3, and (c) ZAO-6.

Table 2. Surface roughness parameters of $ZnAl_2O_4$:SnO_2 thin films.

ZnO Sample ID	Ra (nm)	Rq (nm)	Grain Size (nm)	Surface Description
Undoped	9.4	12.1	78	Smooth and compact surface with fine grains
3 wt% SnO_2	10.6	13.4	71	Uniform grain distribution, moderate roughness
6 wt% SnO_2	11.2	14.0	66	Coarser surface with larger grain clusters

Figure 5 shows the electrical response of $ZnAl_2O_4$ thin films with and without SnO_2 addition at room temperature. The measurements were carried out in the frequency range of 75 kHz to 1 MHz, and the results show that all samples exhibit a characteristic semicircular behavior, which indicates that the charge transport is mainly controlled by the grain interior of the films.

The diameter of each curve represents the overall resistance of the material, while the slope near the high-frequency end reflects the capacitive behavior of the film. It is observed that the curves for the doped samples are smaller compared with the undoped one, meaning that the total resistance decreases as SnO_2 is introduced. This behavior suggests an improvement in electrical conductivity due to the presence of Sn^{4+} ions and the formation of additional oxygen vacancies within the oxide network [30].

The extracted electrical parameters are listed in Table 3. The resistance (R_p) values decreased from about 75.9 Ω for the undoped film to 51.9 Ω for the 3 wt% SnO_2 sample and 56.2 Ω for the 6 wt% SnO_2 sample. At the same time, the capacitance increased from 2.69 nF to approximately 5.9 nF, indicating better charge storage and polarization capability in the doped films. These results confirm that SnO_2 enhances the charge transport pathways within the $ZnAl_2O_4$ matrix, which may be beneficial for sensor or dielectric applications.

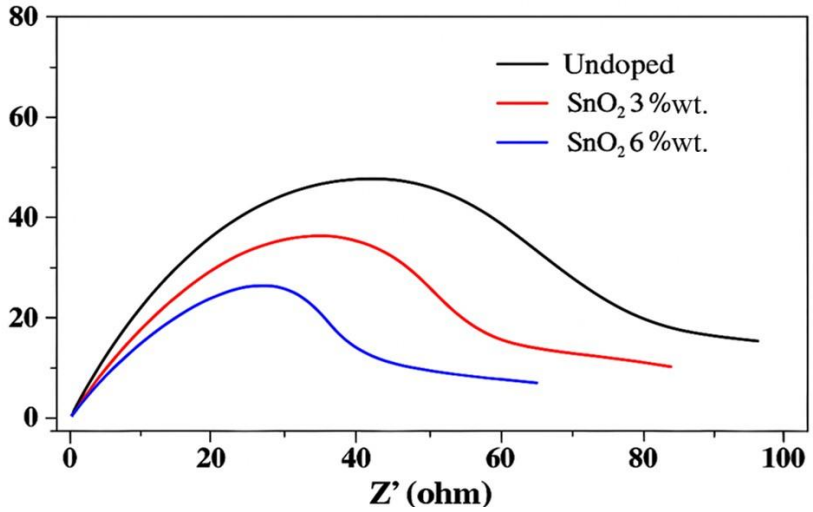

Fig. 5 The electrical response of $ZnAl_2O_4$ thin layers with undoped and SnO_2-doped compositions, where the frequency varies from 75 kHz to 1 MHz at ambient temperature

Table 3. Electrical parameters of $ZnAl_2O_4$:SnO_2 thin films obtained from the fitted curves.

ZnO Sample ID	R_p (Ω)	C (nF)	f_{max} (kHz)	Observation
Undoped	75.9	2.69	770	High resistance, low capacitance
3 wt% SnO_2	51.9	5.95	525	Lowest resistance, highest capacitance
6 wt% SnO_2	56.2	5.59	510	Slight increase in resistance compared to ZAO-3

Conclusion

In this study, $ZnAl_2O_4$:SnO_2 composite thin films were successfully prepared using a simple sol–gel dip-coating method followed by a two-step annealing process. The obtained results confirm that the preparation route is reliable and reproducible for producing uniform and crack-free coatings without the need for a vacuum system.

FTIR spectra verified the formation of the Zn–O–Al vibration band near 655 cm^{-1}, while XRD analysis revealed that all samples maintained a single cubic spinel $ZnAl_2O_4$ phase with no secondary SnO_2 peaks. The addition of SnO_2 slightly reduced the crystallite size from about 25 nm to nearly 22 nm, indicating minor lattice strain. AFM images showed smooth surfaces with homogeneous grain distribution, and the roughness increased slightly with SnO_2 concentration.

The optical measurements confirmed that the films are highly transparent in the visible range, with a small redshift of the absorption edge upon SnO_2 addition, leading to a minor decrease in the band gap from 3.80 eV to 3.68 eV. The electrical results demonstrated that SnO_2 doping decreased the total resistance and enhanced the capacitance of the films, suggesting improved charge transport and dielectric behavior.

Overall, the study demonstrates that combining $ZnAl_2O_4$ with SnO_2 provides a practical way to tune both structural and functional characteristics of spinel-based thin films. These features make the prepared materials potential candidates for future optoelectronic or sensor-related applications..

Author Contributions

All authors mentioned above must have made a significant contribution to the work. EX: A.B. designed the study; C.D. conducted experiments; E.F. analyzed the data; A.B. and E.F. wrote the manuscript… etc.

Funding Statement

Disclosure of any financial support received for this work. Write "Not Applicable" if no funding was received.

Declarations

Consent to publish

Permission to **publish** information that could identify a person (e.g., case reports, photos, videos, voice recordings, distinctive clinical histories, rare diseases). This is **in addition** to consent to participate.

Consent to participate

A statement confirming that all human participants (or their legal guardians) agreed to take part in the study after being adequately informed (i.e., informed consent). This is **separate** from permission to publish identifiable information.

Conflicts of Interest

This is mandatory for all authors submitting to JUAPS. Disclose any potential conflicts (financial, personal, academic, etc.).

EX: "The authors declare no competing interests." Or you should declare if there is any.

Ethical Approval and Consent

Approval number and date from the committee are required for studies involving human or animal subjects. Also, state if written or verbal consent was obtained from the human participant.

Write "Not Applicable" if there are none.

References

Times New Roman 11 pt (1.5 space). **Vancouver style**

DOI is required in full as shown below.

Google Scholar links are needed for all references.

1. A.Q. Tuama, Thermal Diffusivity Nanocomposites of UPE/Nano-Magnesium Oxide, ResearchGate, 2021.
2. A.Q. Tuama, Surface Hardness Modify and Improve Wear Properties of EP/Nano-ZrO_2, ResearchGate, 2021.
3. A.Q. Tuama, Improving the Wear-Resisting of Dry-Slide Friction of Novolac–Graphene Nanocomposites, ResearchGate, 2023.
4. M. Sun, X. Zhang, Y. Liu, J. Alloys Compd., 928 (2022) 167183.
5. R. Dhananjay, P. Patil, Appl. Surf. Sci., 533 (2020) 147473.

6. K.L. Foo, U. Hashim, Mater. Chem. Phys., 216 (2018) 170–180.
7. P.S. Patil, Sens. Actuators B: Chem., 285 (2019) 345–353.
8. S.B. Sadale, A.M. Patil, Thin Solid Films, 636 (2017) 118–124.
9. H.A. Gharibshahi, S. Othman, J. Mater. Sci.: Mater. Electron., 32 (2021) 11044–11056.
10. L. Zheng, J. Wang, Ceram. Int., 49 (2023) 28902–28910.
11. C. Liu, D. Wu, J. Mater. Sci., 57 (2022) 12166–12180.
12. R. Ghosh, P. Mukherjee, Surf. Coat. Technol., 372 (2019) 291–298.
13. M.S. Suresh, A. Rao, J. Sol–Gel Sci. Technol., 100 (2021) 229–239.
14. A. Arunkumar, R. Rajendran, Ceram. Int., 49 (2023) 28902–28910.
15. T.K. Mandal, P.K. Sahoo, Sens. Actuators B: Chem., 368 (2022) 132031.
16. M. Rahman, N. Uddin, J. Mater. Sci., 57 (2022) 12166–12180.
17. H. Zhang, Y. Li, J. Phys. Chem. Solids, 167 (2022) 110707.
18. S. Rao, A. Banerjee, Appl. Phys. A, 128 (2022) 763.
19. P. Kumar, S. Chaudhari, Mater. Today Proc., 65 (2023) 2663–2669.
20. F. Li, L. Tang, Electrochim. Acta, 404 (2022) 139707.
21. M. Jiang, H. Liu, J. Mater. Sci.: Mater. Electron., 33 (2022) 16433–16441.
22. A. Banerjee, S. Rout, Phys. B Condens. Matter, 651 (2022) 413295.
23. D. Patel, V. Chawla, J. Non-Cryst. Solids, 585 (2022) 121528.
24. J. Wang, L. Huang, CrystEngComm., 25 (2023) 3786–3798.
25. R. Chen, M. Chen, J. Eur. Ceram. Soc., 42 (2022) 5928–5936.
26. G. Li, C. Zhang, J. Mater. Sci. Eng. B, 278 (2023) 115643.
27. N. Das, A. Pal, Adv. Mater. Res., 1221 (2023) 72–80.
28. M. Ahmed, T. Hassan, Appl. Surf. Sci. Adv., 15 (2023) 100387.
29. Y. Kim, J. Lee, Ceram. Int., 49 (2023) 32714–32723.
30. F.K. Farhan, A.Q. Tuama, Thermal and Structural Behavior of $MgSO_4$-Doped Phosphate Glass for Biomedical Applications, Manuscript in Preparation, 2025.